

Electrical conductivity of hydrous basaltic melts: implications for partial melting in the upper mantle

Huaiwei Ni · Hans Keppler · Harald Behrens

Received: 9 November 2010 / Accepted: 9 February 2011 / Published online: 24 February 2011
© Springer-Verlag 2011

Abstract The Earth's uppermost asthenosphere is generally associated with low seismic wave velocity and high electrical conductivity. The electrical conductivity anomalies observed from magnetotelluric studies have been attributed to the hydration of mantle minerals, traces of carbonatite melt, or silicate melts. We report the electrical conductivity of both H₂O-bearing (0–6 wt% H₂O) and CO₂-bearing (0.5 wt% CO₂) basaltic melts at 2 GPa and 1,473–1,923 K measured using impedance spectroscopy in a piston-cylinder apparatus. CO₂ hardly affects conductivity at such a concentration level. The effect of water on the conductivity of basaltic melt is markedly larger than inferred from previous measurements on silicate melts of different composition. The conductivity of basaltic melts with more than 6 wt% of water approaches the values for carbonatites. Our data are reproduced within a factor of 1.1 by the equation $\log \sigma = 2.172 - (860.82 - 204.46 w^{0.5}) / (T - 1146.8)$, where σ is the electrical conductivity in S/m, T is the temperature in K, and w is the H₂O content in wt%. We show that in a mantle with 125 ppm water and for a bulk water partition coefficient of 0.006 between minerals and melt, 2 vol% of melt will account for the observed electrical conductivity in the seismic low-velocity zone. However, for plausible higher water contents, stronger water partitioning into the melt or melt segregation in tube-

like structures, even less than 1 vol% of hydrous melt, may be sufficient to produce the observed conductivity. We also show that ~1 vol% of hydrous melts are likely to be stable in the low-velocity zone, if the uncertainties in mantle water contents, in water partition coefficients, and in the effect of water on the melting point of peridotite are properly considered.

Keywords Basaltic melt · Hydrous melt · Electrical conductivity · Partial melting

Introduction

Magnetotelluric studies have revealed regions with high electrical conductivities (>0.1 S/m) in the Earth's uppermost asthenosphere (Evans et al. 2005; Baba et al. 2006), which roughly corresponds to the seismic low-velocity zone (LVZ) at 70–220 km depths. Furthermore, electrical conductivity shows a marked anisotropy in the oceanic LVZ, with higher values in the direction of plate spreading.

The electrical conductivity of anhydrous olivine is lower than 0.01 S/m under LVZ pressure–temperature conditions (Xu et al. 1998; Constable 2006). As a result, hydrated olivine was proposed to cause the conductivity anomalies in the LVZ (Wang et al. 2006; Karato 2006). However, it appears from recent conductivity measurements on olivine single crystals (Yoshino et al. 2006; Poe et al. 2010) that hydrated olivine cannot account for the high conductivity or the electrical anisotropy.

Another possibility to enhance mantle conductivity is partial melting, as silicate melts have long been known to be more electrically conductive than solid silicates (Presnall et al. 1972). Although MORB is primarily produced in the upper ~65 km of the oceanic lithosphere

Communicated by J. Hoefs.

H. Ni (✉) · H. Keppler
Bayerisches Geoinstitut, Universität Bayreuth,
95440 Bayreuth, Germany
e-mail: Huaiwei.Ni@Uni-Bayreuth.DE

H. Behrens
Institut für Mineralogie, Leibniz Universität Hannover,
Callinstr. 3, 30167 Hannover, Germany

(Shen and Forsyth 1995), constraints from trace elements partitioning suggest that very low degree of silicate melting (<1%) initiates in the garnet peridotite field (Salters and Hart 1989), probably below 100 km depth. However, based on the conductivity of anhydrous basaltic melts, Tyburczy and Waff (1983) showed that a melt fraction of at least 5–10% is necessary to match the observed anomalies. Therefore, there appears to be a discrepancy between geochemically and geophysically inferred melt fractions.

This discrepancy could be settled by assuming a carbonatite melt instead, which is extremely conductive (Gaillard et al. 2008). However, there is a sharp contrast between the low CO₂ content of the MORB source mantle (about 72 ppm CO₂; Saal et al. 2002) and the tremendously high CO₂ content in carbonatite melts (typically 30–45 wt%). Even if one assumes that the entire carbon in the MORB source were converted into carbonatite melt, this would only yield a melt fraction of <0.024%, four times lower than the value of 0.1% estimated by Gaillard et al. (2008) to be necessary to explain the observed conductivity. Furthermore, recent measurements at 3 GPa (Yoshino et al. 2010) yield lower electrical conductivities for carbonatite melt than previously measured at atmospheric pressure (Gaillard et al. 2008). In addition, silicate melt rather than carbonatite melt has been advocated to be present at <180 km depths (Hirschmann 2010).

Water is known to have a dramatic effect on thermodynamic and transport properties of silicate melts (e.g., Shaw 1963; Watson 1979; Ochs and Lange 1997; Zhang et al. 2010). Particularly, electrical conductivities of silicate melts are significantly increased with the presence of a few weight percent dissolved H₂O (Gaillard 2004; Pommier et al. 2008; Ni et al. 2011). Therefore, the high electrical conductivities observed in the LVZ may be related to coexisting hydrous silicate melts. Moreover, hydrous silicate melting is likely to generate an electrical signature in subduction zones (Soyer and Unsworth 2006; Brasse et al. 2009) that are widely known for water-induced melting of mantle wedges.

To assess the influence of H₂O on the conductivity of silicate melts and partially molten mantle, we have carried out an experimental investigation on the electrical conductivity of hydrous basaltic melts. Impedance spectra were collected at 1,473–1,923 K and 2 GPa in a piston-

cylinder apparatus. We placed emphasis on the temperature and H₂O dependences of the electrical conductivity, but the effect of small amount of dissolved CO₂ was also examined.

Experimental methods

Starting material

Anhydrous basaltic glass was synthesized by fusing oxides and carbonates at 1,873 K in a chamber furnace at ambient pressure. The glass, quenched by placing Pt crucible in a water bath, was crushed and melted again to ensure homogeneity. Its composition (Table 1) was aimed to represent the near-solidus partial melt at 1,633 K and 1.5 GPa for an asthenospheric mantle (Falloon et al. 2008). To avoid complexities related to iron (multivalency, reduced glass transparency, iron loss to platinum), Fe was replaced with Mg and Ca while keeping the same Mg/Ca ratio. The electrical conductivity of this haplobasaltic melt is not much different from that of natural basaltic melts, as will be shown later. The anhydrous glass is free of bubbles or crystals, but contains 0.02 wt% residual water based on FTIR analysis.

Mixtures of anhydrous glass powder and water were sealed in Pt capsules, and hydrous glasses were synthesized at 1,623 K and 0.3–0.4 GPa for 3 h in an internally heated pressure vessel at Universität Hannover. Run products are transparent glasses except for the one with ~6 wt% H₂O, which is partially crystalline. Water contents of the hydrous glasses are 1.1, 4.1, and 6.3 wt%, as measured with the Karl Fischer Titration (KFT) method. Examining the two ends of the hydrous glass with 4.1 wt% H₂O showed a slight H₂O gradient, with ~15% variation across ~25 mm (length of the sample). Water contents of the glasses were also checked with a Bruker IFS 120HR FTIR spectrometer. Based on the water contents quantified by KFT, the linear molar absorptivity was determined to be 0.056 L/mol/mm for the 5,220 cm⁻¹ molecular H₂O band and 0.049 L/mol/mm for the 4,500 cm⁻¹ OH band using two tangential lines as baselines. These values are similar to those determined for a Fe-bearing basaltic glass (Ohlhorst et al. 2001).

Table 1 Composition of anhydrous haplobasaltic glass in wt%

SiO ₂	TiO ₂	Al ₂ O ₃	MnO	MgO	CaO	Na ₂ O	Cr ₂ O ₃	Total	H ₂ O	Comment
50.06	1.27	17.94	0.11	13.24	13.32	3.67	0.12	99.73	0.02	Before run
49.90	1.15	19.62	0.05	12.99	13.08	3.54	0.02	100.35	0.03	After run

Oxides contents (averages of 30 analyses) are determined by a JEOL JXA-8200 electron microprobe with a beam of 15 kV, 15 nA, and 5 μm diameter. H₂O content is measured by FTIR for the 3,550 cm⁻¹ band using the calibration of Yamashita et al. (1997) for a tholeiitic melt. The “after run” composition is for the sample after the run HBS-dry-EC5

A CO₂-bearing glass was synthesized at 1,823 K and 2 GPa for 10 min in a piston-cylinder apparatus at BGI, following the method developed by Korschak (2008). Anhydrous glass powder was sealed in a Pt capsule, together with silver oxalate (Ag₂C₂O₄), Ag₂O, and a piece of gold. Ag₂O was used to maintain high oxygen fugacity and to prevent graphite formation. Upon heating, silver oxalate decomposed to CO₂ (dissolved into the melt) and silver droplets (which alloyed with the molten gold piece), as pointed out by Korschak (2008). The product was a transparent haplobasaltic glass with 0.3 wt% H₂O (as measured by FTIR spectroscopy) and 0.5 wt% CO₂ (as calculated from the weight of glass powder and silver oxalate).

Conductivity measurements

Anhydrous and hydrous glasses were prepared as cylinders of ~4 mm length and ~3.1 mm diameter. A central hole of 0.5 mm diameter was then drilled along the cylindrical axis of glass using a tungsten carbide drill. The CO₂-bearing glass was ground into powder and cold-pressed into a glass cylinder of a similar shape.

Electrical conductivity measurements were carried out at 2 GPa in a 3/4" piston-cylinder apparatus. A sketch of the sample assembly is illustrated in Fig. 1. The glass cylinder was sandwiched between two ceramic disks (as insulating spacers) at top and bottom. Furthermore, the glass cylinder was bracketed by a Pt rod of 0.5 mm diameter (as the inner electrode) and a Pt₉₅Rh₅ tube of 3.2 mm inner diameter (as the outer electrode). Compared to pure Pt, Pt₉₅Rh₅ alloy has higher hardness and strength at high temperature, which makes it ideal for retaining sample geometry. Moreover, the rhodium content suppresses recrystallization of the platinum at high temperature and therefore reduces water loss. The small difference in electrode compositions is not expected to have a significant effect on conductivity measurements. The Pt₉₅Rh₅ tube was welded at one end and sealed with boron nitride at the other end. The two electrodes were connected to a Solartron 1260 impedance analyzer using Pt wires of 0.35 mm diameter (referred to below as EC wires). Analyzer performance was always verified by measuring a Solartron 12861 test module before and after experiment. Pressure medium was crushable Al₂O₃ inside the graphite heater and talc and Pyrex glass outside the heater. In addition, we used a Mo foil of 0.125 mm thickness to shield the conductivity measurements from the inductive effects of the heating circuit.

Each sample assembly was kept at 423 K in a furnace overnight and then heated to 773 K for 15 min, to remove moisture and reduce background conductivity. Next, the assembly was loaded into the piston-cylinder apparatus

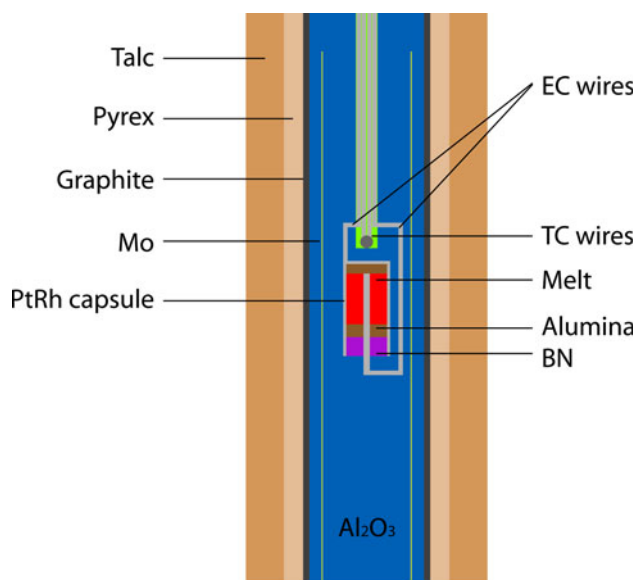


Fig. 1 Sketch of sample assembly for electrical conductivity measurements in a piston-cylinder apparatus (drawn to scale). The assembly contains graphite as heater and talc–Pyrex glass–crushable alumina as pressure medium. Electrical conductivity of the basaltic melt is measured between a platinum (Pt) rod as the inner electrode and a Pt₉₅Rh₅ capsule as the outer electrode, which are led out with two platinum wires (EC wires). Temperature is monitored by a Pt–Pt₉₀Rh₁₀ thermocouple (TC wires). Ceramic alumina and boron nitride (BN) are used as insulation spacers. A molybdenum (Mo) foil shields EC measurements from electromagnetic induction by the heating circuit

and piston-in compressed to 2 GPa (with 9% correction on nominal pressure). Temperature was monitored using a Pt–Pt₉₀Rh₁₀ thermocouple, which was not involved in the circuit of conductivity measurements. The thermocouple was only ~1 mm above the top of the melt; therefore, measured temperatures are reported without any correction for temperature gradients. We applied stepwise heating and measured the electrical conductivity at each temperature using an ac voltage of 1 V sweeping from 3 MHz to 3 Hz. Only the superliquidus data are of interest here and are reported. At such temperatures, impedance reached steady state within a few minutes. Density estimates based on Lange and Carmichael (1987) indicate that melt should expand by less than 4% from 298 to 1,923 K and by less than 2% in the temperature range of interest. Therefore, thermal expansion should not affect cell geometry much and will not be further considered.

The glass sample was replaced with ceramic alumina to evaluate the background conductivity, which turned out to be about two orders of magnitude lower than melt conductivity. On the other hand, since we used a two-electrode instead of a four-electrode setup (four-electrode measurements are extremely challenging in high-pressure devices),

the EC wires should contribute to measured impedance, as pointed out by Gaillard et al. (2008) and Pommier et al. (2010a). To evaluate wire contribution, we have performed a short-circuit experiment, in which the inner Pt rod and the Pt₉₅Rh₅ capsule are in direct contact.

After impedance acquisitions, quenched samples were mounted into epoxy resin and doubly polished to sections of 1 mm thickness. Images of one sample cell and the short-circuit cell were recorded under an optical microscope (Fig. 2). Samples did not suffer much deformation, and their original geometry was largely preserved. The interfaces between the alumina spacers and the melt remained sharp, indicating no sign of interface reaction. Anhydrous melt composition exhibited little change (Table 1). However, despite that minimal dwelling time at high temperatures, FTIR measurements demonstrated H₂O loss for the hydrous samples (Table 2), especially the one that experienced two cycles of heating and cooling (HBS-H4-EC1). Experimental details are summarized in Table 2.

Results and discussion

Impedance spectra and resistance

Examples of impedance spectra are shown in Fig. 3 as Argand diagrams. The shape of the spectra is similar to those reported by Pommier et al. (2008) and Gaillard et al. (2008). The high-frequency region at positive Z'' is due to EC wire inductance, whereas the low-frequency region at negative Z'' is due to the response of sample–electrode

interface. The dc resistance can be found from the Z' intercept (where $Z'' = 0$) of the spectra.

The contribution from EC wires needs to be removed from dc resistance. In the short-circuit experiment, wire resistance increased from $\sim 1.2 \Omega$ at 298 K to $\sim 1.6 \Omega$ at 1,923 K (Fig. 4). Accordingly, real melt resistance R at a given temperature T can be found as follows:

$$R(T) = R'(T) - R_{SC}(T) - R_{Pt} \quad (1a)$$

$$R_{Pt} = \rho_{Pt298} \frac{\Delta \ell}{S} \quad (1b)$$

where R' is dc resistance, R_{SC} is wire resistance from the short-circuit experiment, R_{Pt} is an additional correction considering different EC wire length in each experiment, ρ_{Pt298} is Pt resistivity at 298 K, $\Delta \ell$ is the length difference (from 0.46 m to 1.04 m) between the Pt wire in the respective experiment and that in the short-circuit experiment, and S is the cross-section area of EC wire. The values of R_{Pt} are given in Table 2. For experiment HBS-dry-EC5, the resistance correction (combining R_{SC} and R_{Pt}) is 14% at 1,723 K and 28% at 1,923 K. For experiment HBS-H6-EC1, the correction is as high as 31% at 1,473 K and 59% at 1,773 K. Note that since EC wire length can be precisely measured (within 1%), R_{Pt} is a calculated property of high accuracy. Therefore, the uncertainties in applying resistance correction are smaller than what appear from the above percentages of total correction (14–59%).

Temperature and H₂O dependences of conductivity

The electrical conductivity can be related to melt resistance through (Barsoukov and Macdonald 2005)

Fig. 2 **a** Image of sample cell HBS-dry-EC5. Deformation is minimal, and the original geometry is largely preserved for the melt cell. No sign of reaction is identified between ceramic alumina and the melt. **b** Image of short-circuit cell, in which the two electrodes are in direct contact

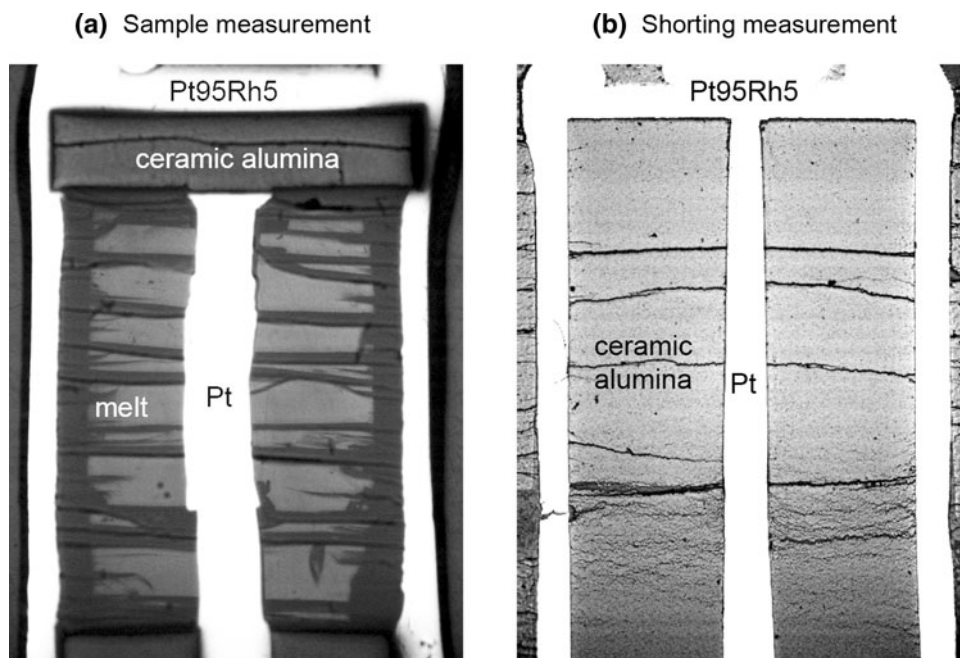


Table 2 Experimental conditions

Run #	H ₂ O		CO ₂ (wt%)	Geometry factor (mm)	T range (K)	R _{PT} ^d (Ω)
	Initial ^a (wt%)	Final ^b (wt%)				
HBS-dry-EC5	0.018 ± 0.004	0.027 ± 0.002	–	14.1	1723–1923	0.68
HBS-H1-EC1	1.1	0.63 ± 0.01	–	14.0	1673–1873	0.84
HBS-H4-EC1	4.1 ± 0.3	1.75 ± 0.01	–	14.2	1573–1873	1.18
HBS-H6-EC1	6.3	4.0 ± 0.1	–	14.1	1473–1773	1.01
CHBS-EC1	0.31 ± 0.01	0.22 ± 0.02	0.5	11.1	1723–1923	0.52

^a Initial H₂O content for HBS-dry and CHBS is determined by FTIR using the calibration of Yamashita et al. (1997), with uncertainties estimated from multiple analyses. Initial H₂O content for the hydrous glasses is determined by KFT (without correction), with the uncertainty for HBS-H4-EC1 estimated from the measurements at two ends of the synthesized glass

^b Final H₂O content is determined by FTIR, with uncertainties estimated from multiple analyses. For hydrous glasses and CHBS, we apply the molar absorptivities for 5,200 cm⁻¹ and 4,500 cm⁻¹ bands derived in this study. HBS-H4 experienced two heating and cooling cycles

^c CO₂ content is calculated from the weight of added dry glass powder and silver oxalate for synthesis

^d Additional resistance correction considering different EC wire lengths

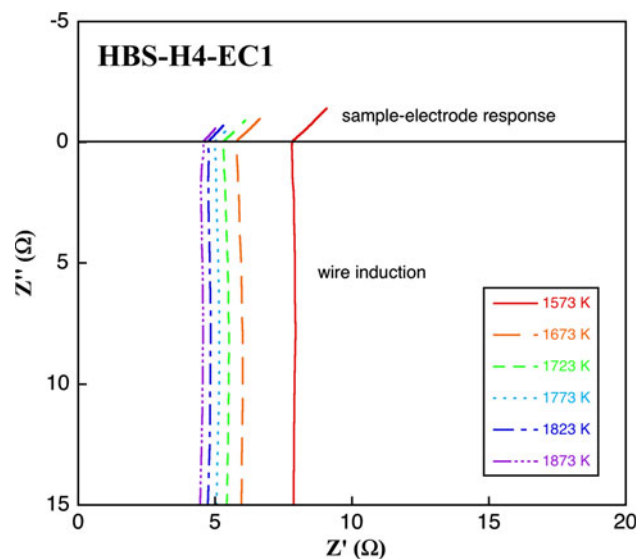


Fig. 3 Impedance spectra (*Argand diagrams*) of the basaltic melt with 4.1 wt% H₂O (HBS-H4-EC1), acquired from 3 M Hz to 3 Hz at 1,573–1,873 K and 2 GPa. The impedances at high frequencies (positive Z'') are due to EC wire induction, and those at low frequencies (negative Z'') are due to the response of sample–electrode interface. Sample resistance can be determined from the Z' intercept of the spectra (where Z'' = 0), which decreases as temperature increases

$$\sigma = \frac{1}{\rho} = \frac{\ln(r_o/r_i)}{2\pi lR} = \frac{1}{RG} \quad (2)$$

where σ is the electrical conductivity, ρ is the melt resistivity, r_o and r_i are the outer radius and the inner radius of the melt, l is the length of the melt, and $G = 2\pi l/\ln(r_o/r_i)$ is the geometry factor (Table 2).

Figure 5a shows the conductivity evolution of the melt initially with 4.1 wt% H₂O during two heating and cooling cycles. The data in a cooling cycle lie below those in the previous heating cycle, apparently due to H₂O loss from

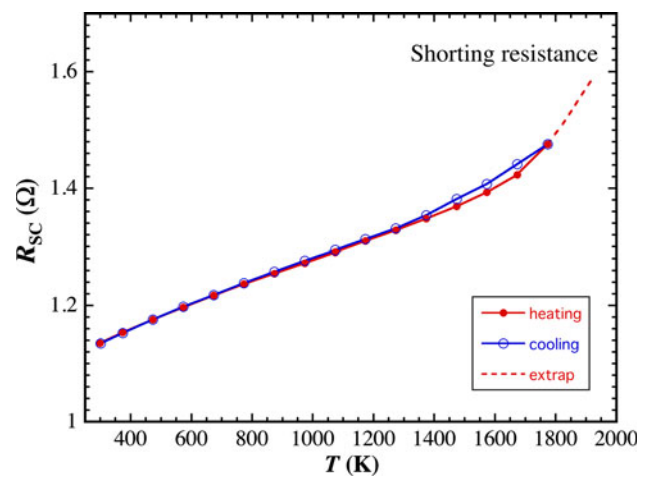


Fig. 4 Resistance variation with temperature acquired from the short-circuit experiment, with extrapolated values given at >1,773 K

the melt at high temperatures. The data in the second heating cycle are close to those in the first cooling cycle below 1,873 K, which suggests that major H₂O loss probably occurred at temperatures above 1,873 K. Therefore, only the data acquired at ≤1,873 K during the first heating cycle are deemed to be the true values for basaltic melt with 4.1 wt% H₂O.

Electrical conductivities of H₂O-bearing basaltic melts during the first heating cycle are presented in Fig. 5b. The conductivity of basaltic melts increases with temperature and H₂O content, qualitatively similar to the corresponding effects for rhyolite melts (Gaillard 2004), phonolite–tephrite melts (Pommier et al. 2008), and albite melts (Ni et al. 2011).

The H₂O dependence of the logarithm of conductivity is weaker than a linear relationship and can be well described with a square root relation. With respect to temperature dependence, we observe a non-Arrhenian behavior of

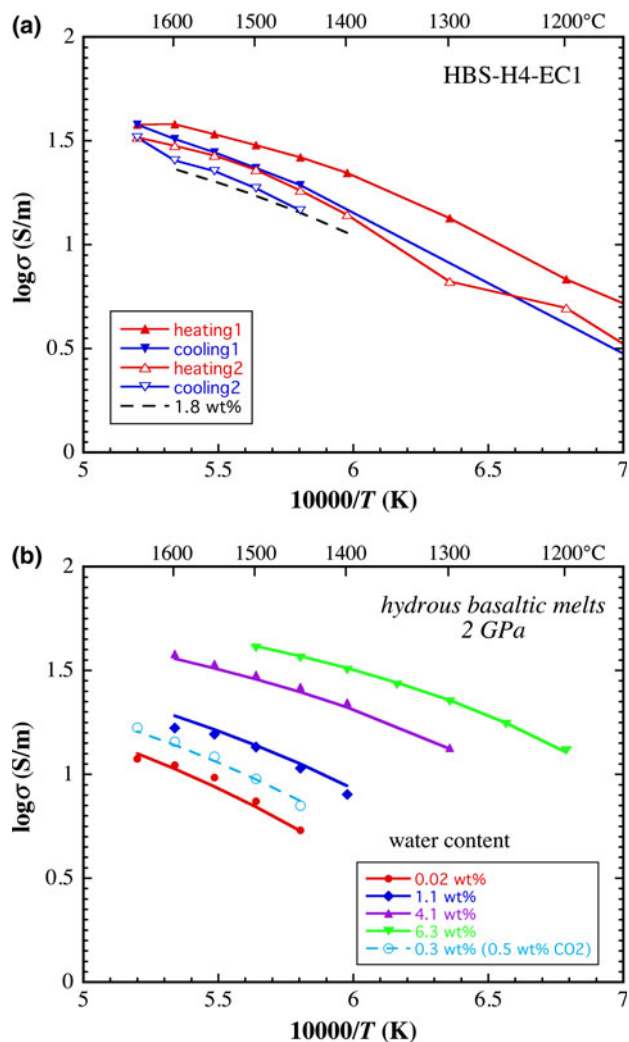


Fig. 5 **a** Electrical conductivity of basaltic melt initially with 4.1 wt% H₂O (HBS-H4-EC1) measured in two heating and cooling cycles. The calculated values (based on Eq. 3) for the melt with 1.8 wt% H₂O (the final H₂O content determined by FTIR) are shown in dashed curve for comparison. **b** Electrical conductivity of hydrated basaltic melts at 2 GPa during first heating. Conductivity increases with temperature and H₂O content but CO₂ does not appear to have a major effect. Curves are fits based on Eq. 3

electrical conductivity, i.e., $\log \sigma$ is not linear with $1/T$. For hydrated melts, the flattened slopes toward higher temperature may be partly due to an increasing H₂O loss, but this cannot explain the same trend for the anhydrous melt. A similar effect for anhydrous basaltic melts was also noted in previous work (Khitarov et al. 1970; Presnall et al. 1972; Murase and McBirney 1973; Waff and Weill 1975; Tyburczy and Waff 1983). The non-Arrhenian behavior may be due to the stronger thermal motion of melt components at high temperature and hence the increased number of collisions of the charge carriers with other atoms. This effect is believed to be responsible for the increasing resistance of metallic conductors with temperature (Lowrie

1997). Alternatively, the deviation from the Arrhenius law may be related to the high fragility of melts (Angell 1991; Pfeiffer 1998), which is inferred from the viscosity–temperature relation of basaltic melts (Giordano and Dingwell 2003).

We adopt the VFT (Vogel-Fulcher-Tammann) equation (Fulcher 1925) to describe the temperature dependence of melt conductivity and obtain the following expression:

$$\log \sigma = 2.172 - \frac{860.82 - 204.46\sqrt{w}}{T - 1146.8} \quad (3)$$

where σ is the electrical conductivity in S/m, T is the temperature in K, and w is the H₂O content in wt%. Experimental data are reproduced by Eq. 3 within a factor of 1.1 (Fig. 5b). The conductivities of the melt with 1.8 wt% H₂O (the final H₂O content in the run HBS-H4-EC1) calculated from Eq. 3 are close to the data acquired during the second cooling cycle (Fig. 5a), which further corroborates the validity of our conductivity expression.

Equation 3 implies that the activation energy, E_a , for electrical conductivity decreases with increasing temperature and increasing H₂O content. The activation energy at a given temperature and H₂O can be calculated by

$$E_a = \frac{\Re T^2 \partial \ln \sigma}{\partial T} \quad (4)$$

where \Re is the gas constant (8.3145 J/mol/K). We found E_a is 98–142 kJ/mol (or 1.02–1.47 eV) for the anhydrous melt at 1,923–1,723 K, 82–125 kJ/mol for the melt with 1.1 wt% H₂O at 1,873–1,673 K, 57–116 kJ/mol for the melt with 4.1 wt% H₂O at 1,873–1,573 K, and 53–136 kJ/mol for the melt with 6.3 wt% H₂O at 1,773–1,473 K.

The CO₂-bearing melt contains 0.3 wt% H₂O, and its conductivities are almost identical to those predicted by Eq. 3. Therefore, the effect of small amounts of CO₂ in the order of 0.5 wt% on electrical conductivity is small compared to the effect of H₂O.

Conduction mechanism

In ionically conducting materials such as silicate melts, the bulk electrical conductivity contains contributions from each ion. Previous work (e.g., Pfeiffer 1998; Gaillard and Iacono-Marziano 2005) demonstrated that electrical conduction should be dominated by the transport of light alkalis (Li and Na) when they are present in silicate melts. Na diffusivity in basaltic melts has an activation energy of ~ 160 kJ/mol at $\sim 1,673$ K (Lowry et al. 1982), which is comparable to the activation energy of 120–150 kJ/mol for the conductivity of a tholeiitic melt (Tyburczy and Waff 1983) or the activation energy for anhydrous basaltic melt from this work (~ 142 kJ/mol at 1,723 K). Hence, we conclude that Na transport is also the dominating

mechanism for electrical conduction in our anhydrous basaltic melt. Assuming other contributions to the electrical conductivity are negligible, the electrical conductivity may be related to Na diffusivity through the Nernst-Einstein relation:

$$\sigma = \frac{1}{H_R} \frac{Dc(zF)^2}{RT} \quad (5)$$

where D is the Na diffusivity, c is the concentration of Na cations, z is the charge (+1 for Na^+), F is the Faraday constant (96,485 C/mol), and H_R is the Haven ratio. The Haven ratio is equivalent to the correlation factor of the diffusion process and is determined by the diffusion mechanism (e.g., vacancy vs. interstitial), as pointed out by Haven and Verkerk (1965). Na diffusivity data in basaltic melt at 2 GPa are not available. To bring the Na diffusivity (Lowry et al. 1982) and the electrical conductivity of basaltic melt at 0.1 MPa (Tyburczy and Waff 1983) in concert with Eq. 5, the Haven ratio should be ~ 0.2 , which is a reasonable factor for silicate melts (Haven and Verkerk 1965; Heinemann and Frischat 1993).

For hydrous melts, one may expect that the positive H_2O effect on electrical conductivity is due to the participation of hydrogen in electrical conduction. However, H_2O diffusion studies (Zhang et al. 1991; Ni and Zhang 2008; Ni et al. 2009a, b) indicate that hydrogen transport is dominated by the neutral H_2O molecule in polymerized melts, although it is less conclusive in depolymerized melts (Zhang and Stolper 1991; Behrens et al. 2004). Under extremely reducing conditions, hydrogen moves in the form of molecular H_2 (Gaillard et al. 2003; Zhang and Ni 2010), still a neutral particle. Furthermore, protons are not energetically stable, and hydrogen in silicate melts is predominantly bonded to oxygen (Ernsberger 1980). The electrical conductivity of alkali-free hydrous glasses was determined to be rather low (e.g., Behrens et al. 2002). Therefore, the positive correlation between electrical conductivity and H_2O content is probably due to enhanced Na mobility, as suggested by Gaillard (2004). H_2O can facilitate Na transport by decreasing melt viscosity and hence accelerating melt dynamics in general (Zhang et al. 2010). In contrast, CO_2 in the order of 1 wt% in basaltic melt (dissolved partially as CO_3^{2-}) has little effect on melt viscosity (Brearley and Montana 1989), and probably does not play an important role for other transport properties either. The carbonate ion may transport electric charge, but it is too large for rapid movement and therefore its contribution to bulk electrical conductivity should be small.

Comparison with previous work

We first compare our results with previous measurements on natural anhydrous basaltic melts (Fig. 6). The data by

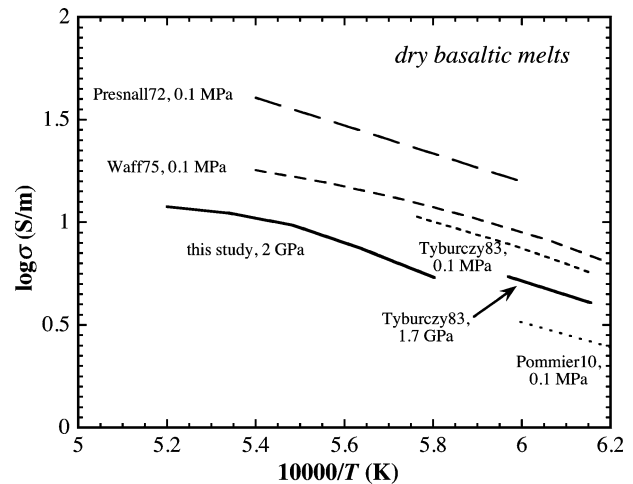


Fig. 6 Electrical conductivities of dry basaltic melts from this study compared with those from previous studies. Data sources: Presnall et al. (1972); Waff and Weill (1975); Tyburczy and Waff (1983); Pommier et al. (2010b)

Presnall et al. (1972) at 0.1 MPa seem to be too high. Pommier et al. (2010b) have reported that reducing oxygen fugacity would enhance conductivity, but their data at 0.1 MPa are very low even at an oxygen fugacity of 10^{-7} bar. The conductivities at 0.1 MPa from Waff and Weill (1975) and Tyburczy and Waff (1983) are similar. They are higher than the conductivities at 2 GPa from this study, consistent with a negative pressure effect. The curve at 1.7 GPa from Tyburczy and Waff (1983) lies only slightly above our data, confirming that Fe-free basaltic melt is a good proxy for natural basaltic melt.

Our results are also compared with previous work on other hydrous silicate melts (Fig. 7). The effect of water is more pronounced in basaltic melts than in other compositions. When ~ 4 wt% H_2O is added to the melt, electrical conductivity increases by a factor of 2–3 in rhyolite (Gaillard 2004), phonolite–phonotephrite (Pommier et al. 2008), and albite melts (Ni et al. 2011), while conductivity increases by a factor of 4–6 in basaltic melt. This trend differs from that observed for viscosity, i.e., the effect of dissolved water is larger for polymerized melts than for depolymerized melts (e.g., Whittington et al. 2000), because water preferentially reacts with bridging oxygen atoms. However, the transport of alkalis, the dominating mechanism for electrical conduction in silicate melts, is not controlled by structural relaxation and not entirely limited by viscosity (Dingwell and Webb 1990; Mungall 2002). In fact, water diffusion, also a process not controlled by structural relaxation, is faster in basaltic melts than in the melts of felsic to intermediate compositions (Zhang and Ni 2010).

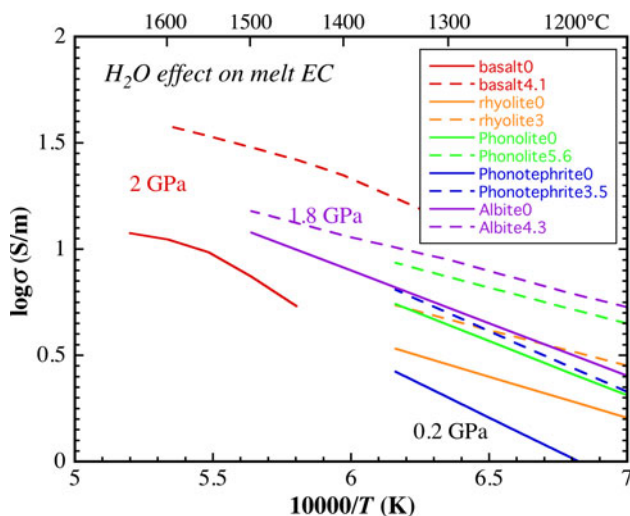


Fig. 7 Compilation of electrical conductivity of both anhydrous and hydrous silicate melts. Data sources: basalt at 2 GPa (this study); rhyolite at 0.2 GPa (Gaillard 2004); phonolite and phonotephrite at 0.2 GPa (Pommier et al. 2008); albite at 1.8 GPa (Ni et al. 2011). The numbers in the legend indicate H₂O contents in wt% for respective melts. H₂O has a larger effect on conductivity of basaltic melt (a factor of 4–6 from 0 to 4 wt% H₂O) than on conductivities of previously investigated melts

Implications for partial melting in the upper mantle

Conductivity of a partially molten upper mantle

The mid-ocean ridge basalt (MORB) source mantle contains 50–200 ppm water, while the enriched mantle of the ocean island basalt (OIB) source contains 500–1,000 ppm (Saal et al. 2002; Kohn and Grant 2006 and the references therein). In subduction zones, water released from the subducted slab triggers melting, leading to high water contents in arc magmas (Sisson and Layne 1993; Grove et al. 2002). When partial melting occurs, water is preferentially partitioned into the melt, and the partition coefficient between mantle and melt ($D_{\text{mant-melt}}$) is between 0.004 and 0.009 from 2 to 7 GPa (Dixon et al. 1988; Bell et al. 2004; Hirschmann et al. 2009). For a low degree of melting (such as 1 vol%), the H₂O content in the melt should be on the order of a few weight percent (corresponding to our investigated compositions).

The electrical conductivity of a partially molten mantle can be estimated using two-phase mixing models (reviewed by Glover et al. 2000). The upper and lower limit is given by the parallel and perpendicular model, respectively. The parallel model corresponds to continuous tubes or sheets of melt, while the perpendicular model would imply isolated pockets of melt. The model based on the Archie (1942)'s law involves free parameters, which have to be predetermined. The Hashin and Shtrikman (1962) upper bound (referred to as HS + below) assumes

that the electrically more conductive phase forms a shell around spherical grains of the less conducting phase. This is a reasonable approximation if the melt is present as interconnected intergranular film. Based on the HS + model, the bulk conductivity (σ) can be calculated from the individual conductivities (σ_1 and σ_2) and the volume fractions (F_1 and F_2) of the two phases (where phase 2 is more conducting):

$$\sigma = \sigma_2 \left[1 - \frac{3F_1(\sigma_2 - \sigma_1)}{3\sigma_2 - F_2(\sigma_2 - \sigma_1)} \right]. \quad (6)$$

Figure 8 displays how electrical conductivity of an H₂O-depleted mantle (with 125 ppm H₂O) and an H₂O-rich mantle (with 600 ppm H₂O) evolves with an increasing degree of melting, at 1,673 K and 2 GPa (roughly the top of asthenosphere following an adiabatic geotherm with a potential temperature of 1,623 K). In the calculation, we assume an average $D_{\text{mant-melt}}$ of 0.006 (Hirschmann et al. 2009) and an electrical conductivity of 0.01 S/m for the solid mantle (Yoshino et al. 2006). The small difference between volume fraction and weight fraction is ignored.

Melting in the oceanic low-velocity zone (LVZ)

In the LVZ below the East Pacific Rise, resistivity models (Evans et al. 2005; Baba et al. 2006) have identified electrical conductivity as high as 0.1 S/m in the direction of plate spreading. High conductivity zones include a horizontal layer (with seafloor ages younger than 5 Ma) at 70–110 km depths and an on-axis region underneath. In the

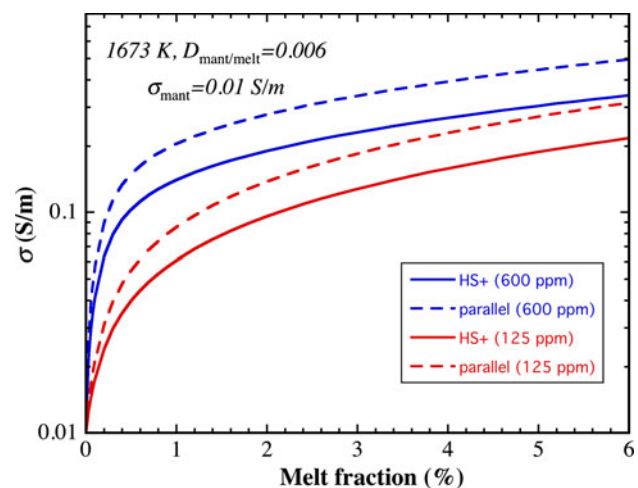


Fig. 8 Electrical conductivity of the mantle (with 600 ppm or 125 ppm H₂O) at different melt fractions, based on the Hashin and Shtrikman (1962) upper bound (HS+) and the parallel model. Calculations assume a partition coefficient of 0.006 for H₂O between the solid mantle and the melt, a temperature of 1,673 K, and a conductivity of 0.01 S/m for the solid mantle

off-axis region at 110–200 km depths, conductivity is lower (~ 0.03 S/m).

For a normal MORB source mantle (with a conservative estimate of 125 ppm H_2O and a bulk partition coefficient of water of 0.006), Fig. 8 indicates that $\sim 2\%$ melting is required to match a conductivity of 0.1 S/m. If the melt was elongated in the direction of plate motion, equivalent to a parallel model, a melt fraction as low as 1.2% would be sufficient. The lower conductivity in off-axis region (0.03 S/m) corresponds to $\sim 0.3\%$ partial melting. The range of melt fractions inferred here from conductivity arguments is entirely consistent with the melt fractions required to explain the seismic contrast at the lithosphere–asthenosphere boundary (0.25–1.25%; Kawakatsu et al. 2009). A partitioning of melt into elongated structures would also be consistent with the conductivity anisotropy, as well as the anisotropy for seismic shear waves (The MELT Seismic Team 1998).

A critical question is whether such hydrous melts are thermodynamically stable in the LVZ. At a depth around 100 km, the temperatures along a ridge geotherm are below the dry solidus of peridotite by roughly 100 K (Hirschmann et al. 2009). Even for an oceanic geotherm with a lithosphere age of 50 Ma, the temperature difference is less than 200 K (Hirschmann et al. 2009). The temperature gaps can be closed by the presence of volatiles. Based on water solubility measurements in mantle minerals, Mierdel et al. (2007) concluded that ~ 100 ppm H_2O is sufficient to induce partial melting in the LVZ. Hirschmann et al. (2009) argued for the necessity of 300–600 ppm H_2O . In a more recent paper, Hirschmann (2010) suggested that the combined effect of water and CO_2 is sufficient to cause silicate melting in the LVZ. For a mantle with 100 ppm H_2O and 60 ppm CO_2 , Hirschmann (2010) inferred 0.1–0.5% melting at depths of 70–110 km and 0.03–0.1% melting underneath. These melt fractions are approximately 5 times lower than our estimates in most of the LVZ, and more than one order of magnitude lower in the on-axis region below 110 km depth. However, we do not consider this discrepancy to be a fundamental problem, because of the many uncertainties involved in predicting the thermodynamic stability of hydrous melts in the mantle. These uncertainties result from potential errors in (1) mantle water contents, (2) water partition coefficients, and (3) the effect of water on solidus temperatures.

The MORB source is usually considered to be representative for the chemical composition of most of the upper oceanic mantle, while the more volatile-rich OIB source probably constitutes a smaller, but not precisely known fraction of this reservoir. The water content in the MORB source can be estimated from the analyses of primitive and undegassed MORB glasses. If the degree of melting that produced these magmas and the bulk partition coefficient

of hydrogen between melt and residual minerals are known, the water content in the source can be calculated. However, because of the considerable uncertainty in these parameters, another approach has been used more successfully in estimating mantle water contents (e.g., Michael 1995; Saal et al. 2002; Workman and Hart 2005). This approach is based on the observation that the $\text{H}_2\text{O}/\text{Ce}$ ratio in MORB glasses is roughly constant, even if the absolute concentrations of these components vary by orders of magnitude (Michael 1995). This implies that H_2O and Ce have nearly the same bulk partition coefficient during the formation of MORB; therefore, the $\text{H}_2\text{O}/\text{Ce}$ ratio in the MORB source must be the same as in the undegassed MORB samples. Together with the relatively well-constrained Ce abundance in the depleted mantle, the observed $\text{H}_2\text{O}/\text{Ce}$ ratio therefore can be used to infer the water content in this reservoir (e.g., Saal et al. 2002). Various estimates based on this method typically yield average upper mantle water contents in the range of 100–200 ppm. However, nearly all data show a considerable scatter in the $\text{H}_2\text{O}/\text{Ce}$ ratio that translates into a significant uncertainty in estimated water concentrations. Saal et al. (2002) observed a $\text{H}_2\text{O}/\text{Ce}$ ratio of 168 ± 95 that translates into a mantle water content of 142 ± 85 ppm. However, both the data of Saal et al. (2002) and the extensive compilation of Michael (1995) show a continuous range of $\text{H}_2\text{O}/\text{Ce}$ ratios from 100 to 350 that will translate into a proportional spread of estimated mantle water contents. In particular, the glasses from the northern part of the Middle Atlantic Ridge appear to have high $\text{H}_2\text{O}/\text{Ce}$ ratios (Michael 1995), suggesting extensive local variations in mantle water content. Moreover, water contents in MORB may not directly reflect the source, but they may have been affected by reequilibration with the surrounding mantle during the upward percolation of the melts. This is plausible, since the diffusion coefficients of water in minerals are orders of magnitude faster than those of other trace elements (Ingrin and Blanchard 2006). Mierdel et al. (2007) have shown that the water solubility in orthopyroxene and in the bulk mantle drastically increases at shallow depths, while water solubility in silicate melts decreases. This should cause water to be repartitioned from the melt into the surrounding mantle upon ascent and such a process may be responsible for the observed variation in the $\text{H}_2\text{O}/\text{Ce}$ ratio. This would imply that actually the higher $\text{H}_2\text{O}/\text{Ce}$ ratios observed are more representative for the MORB source, which would effectively double the estimated water contents for the depleted mantle.

Most water partition coefficients between mantle minerals and melts have been measured using SIMS (secondary ion mass spectrometry), since the crystals obtained in such experiments are usually too small for polarized infrared spectroscopy. However, Kohn and Grant (2006)

pointed out that any non-spectroscopic technique such as SIMS cannot distinguish between water truly dissolved as point defects in a mineral and water in submicroscopic melt inclusions, lamellae of other phases and similar impurities. Measurements by SIMS therefore strictly provide only upper limits of water contents in minerals and of mineral/melt partition coefficients. In the calculations above, we used a bulk partition coefficient between the mantle and the coexisting melt of 0.006, as derived by Hirschmann et al. (2009), for a pressure of 3–4 GPa. However, the error analysis provided by Hirschmann et al. (2009) suggests that partition coefficients down to 0.004 may be consistent with the purely statistical uncertainty in measured partition coefficients. Independent estimates from water solubility measurements suggest even lower values. According to Mierdel et al. (2007), the bulk water solubility in upper mantle minerals along an oceanic geotherm has a minimum of 750–1,000 ppm around 3 GPa, while the water solubility in a basaltic melt at these conditions very likely exceeds 30 wt% (Hodges 1974). This translates into a bulk mantle/melt partition coefficient of water of 0.003 or less.

The effect of low water activities on the solidus temperatures of the mantle has never been directly measured (compare Liu et al. 2006) and even published water-saturated solidus temperatures of the mantle differ by several hundred Kelvin (Grove et al. 2006; Green et al. 2008). This is related to experimental difficulties in detecting low-degree partial melts that usually crystallize during quenching if they contain some water. Distinguishing quenched melt from material precipitated from a fluid upon quenching can be another problem. In the absence of direct experimental data, Hirschmann et al. (2009) and Hirschmann (2010) used a cryoscopic approach to estimate the melting point depression caused by water. This approach, however, only considers the dilution of oxygen atoms in the silicate melt by OH groups. It does not account for the fact that in the presence of water, the composition of the partial melt changes, which by itself changes the melting temperatures (e.g., Kushiro 1972; Gaetani and Grove 1998). These effects will be very strong at low melt fractions, because, here, highly incompatible elements such as potassium will strongly partition into the melt. We note that the model of Hirschmann (2010) is not calibrated at all against true solidus temperatures of a mantle peridotite; it is only calibrated against liquidus temperatures and against melting temperatures corresponding to relatively large melt fractions. The curve used by Hirschmann (2010; their Fig. 3) would predict that a melting point depression of 150 K—a typical value required to stabilize hydrous silicate melts in the LVZ—requires 5 wt% of water in the melt. However, the majority of the experimental data compiled by Hirschmann et al. (2009) suggests a much larger melting point depression for low melt water contents in the range up

to 5 wt% than predicted by the regression curve used by Hirschmann (2010) to infer the stability of hydrous melts in the upper mantle.

To illustrate the feasibility of stabilizing small fractions of hydrous melt in the depleted upper mantle, we have calculated the melt fractions required to explain an electrical conductivity of 0.1 S/m for a mantle containing 227 ppm of water. This is within two standard deviations of the water content inferred by Saal et al. (2002; 142 ± 85 ppm). Assuming a bulk partition coefficient of water of 0.003, as suggested above, we obtain a melt fraction of 1.4% in the HS + model and of 0.66% in the parallel model. The calculated water contents in the melt are 1.4 wt% in the former and 2.4 wt% in the latter case. According to the experimental data compiled in Hirschmann et al. (2009), there are several experimental studies suggesting that a melt water content in the order of 2.4 wt% will produce a melting point depression of 150 K that is close to the required value. The presence of carbon will generate an additional reduction in the melting point and additional albeit smaller contributions may result from other volatile elements such as sulfur (146 ppm) and fluorine (16 ppm; Saal et al. 2002). We therefore conclude that small fractions of hydrous partial melts can explain the electrical conductivity and the low seismic velocities observed in the upper oceanic mantle. These melts may be thermodynamically stable, if the uncertainties in mantle water contents, partition coefficients, and experimentally determined melting point depressions are properly considered.

The suggestion of Gaillard et al. (2008) that traces of carbonatite melt are responsible for the high conductivity in the LVZ appears plausible in the light of the very high conductivities for pure carbonatite melts measured at 0.1 MPa. However, according to recent data by Yoshino et al. (2010), the conductivity of carbonatite coexisting with silicates is probably significantly reduced, because of the intrinsic pressure effect on conductivity and because natural carbonatites will contain some dissolved silica. As pointed out earlier, a main argument against carbonatites as being responsible for the high electrical conductivity in the asthenosphere is the low abundance of carbon in the MORB mantle (72 ± 19 ppm CO_2 , Saal et al. 2002; 36 ± 12 ppm, Salters and Stracke 2004; 50 ± 12 ppm, Workman and Hart 2005) combined with the high carbon content in carbonatites (30–45 wt%), implying that only a very small fraction of carbonatite (0.024%) can be produced, even if all carbon is sequestered in the melt. This fraction is below the values of 0.1% required to explain the observed conductivity in the asthenosphere (Gaillard et al. 2008). Furthermore, carbonatite melts are probably not thermodynamically stable in the seismic low-velocity zone, since at the temperatures prevailing there, they would react

with the mantle peridotite to produce carbon-bearing silicate melts (Hirschmann 2010). Much higher carbon contents than those considered here have sometimes been inferred from analyses of “popping rock” samples. However, as pointed out by Saal et al. (2002), these rocks have the same CO_2/Nb ratio as normal MORB samples; they therefore simply reflect simultaneous enrichment of incompatible trace elements either by very low degrees of melting or by fractional crystallization. If the CO_2/Nb ratios of these rocks are extrapolated to the mantle Nb content, CO_2 concentrations in the depleted upper mantle below 100 ppm are typically obtained. We therefore conclude that the permissible fraction of carbonatite melt in the upper mantle is probably below the threshold required to explain the observed electrical conductivity and it is certainly far below the melt fraction required to explain the drop in shear wave velocity at the lithosphere–asthenosphere boundary (0.25–1.25%; Kawakatsu et al. 2009).

Our data show that 0.5 wt% carbon does not cause any measurable increase in the conductivity of basaltic melts. Alkaline silicate melts may dissolve very large amounts of carbon (>10 wt% at upper mantle pressures; Brooker et al. 2001), but if such carbon-rich silicate melts were present in the upper mantle, the corresponding melt fraction would again be limited by the very low bulk carbon abundance. Although we cannot exclude that high concentrations of CO_2 may have some measurable effect on the electrical conductivity of silicate melts, the absence of an effect for 0.5 wt% of CO_2 and the low bulk abundance of carbon make it unlikely that CO_2 in silicate melts contributes significantly to the observed high electrical conductivities in the seismic low-velocity zone.

Yoshino et al. (2010) suggested that already as little as 1% of anhydrous basaltic melt may explain the observed conductivity in the LVZ. However, they assumed a conductivity of dry basaltic melt of 10 S/m several times higher than according to our measurements and to those Tyburczy and Waff (1983) at 1.7 GPa. Such high conductivities may occur in basaltic melts at 0.1 MPa, but at LVZ pressures, the conductivity will be reduced. To obtain the conductivity in the LVZ, 4% of dry basaltic melt would be required according to our measurements. Such a large fraction of melt would probably not be mechanically stable. Moreover, in the absence of volatiles, melting in the LVZ is certainly not possible.

It is worth noting that for a mantle enriched in volatiles (such as 600 ppm H_2O and 400 ppm CO_2), i.e., the source for enriched MORB or OIB, only 0.5% melting (using the HS + model) or 0.2% melting (using the parallel model) is necessary to match bulk conductivity of 0.1 S/m, and only 0.05% melting reaches 0.03 S/m (Fig. 8). This is because basaltic melt with >6 wt% of water is extremely conductive, approaching carbonatite melt at high pressure.

Melting at subduction zones

Electrical conductivities as high as 0.03–1 S/m have been reported from magnetotelluric studies for the mantle wedge above subducted slabs in a depth of 80–150 km (Soyer and Unsworth 2006; Brasse and Eydam 2008; Brasse et al. 2009). This observation is consistent with the formation of hydrous magmas triggered by H_2O released from the subducted slab, although the high conductivity structure is displaced toward the backarc, roughly 40–100 km away from the volcanic front. The nature of the conductive phase in mantle wedges (whether a fluid or a melt) is still debated (Manning 2004; Grove et al. 2006). Analyses of melt inclusions trapped at pressures up to 0.6 GPa suggest that primitive arc basalts have water contents in the order of 3.0–5.2 wt% (Cervantes and Wallace 2003).

The conductivity of the solid mantle in the backarc is typically 0.01 S/m based on MT inversions (Brasse and Eydam 2008; Brasse et al. 2009). The bulk conductivity of a partially molten mantle wedge will depend on temperature, melt H_2O content, and melt fraction. Our conductivity model of hydrous basaltic melt can be used to place some constraints on these parameters, assuming that the anomalies are caused by low fractions of basaltic melt, rather than by aqueous fluids. The thermal structure of subduction zones is not well resolved, but the temperature at the hot core of the mantle wedge is probably 1,573–1,673 K (van Keken et al. 2002; Arcay et al. 2005). In Fig. 9, we show contour plots for conductivities of 0.03, 0.1, 0.3, 1 S/m as function of H_2O contents in the melt (3–6 wt%) and of melt fraction at 1,573 K and 1,673 K. The relatively low conductivity (0.03 S/m as maximum) in the northern Cascadia subduction zone (Soyer and Unsworth 2006) corresponds to a degree of melting not higher than 0.3%. The 0.1 S/m conductivity in northwestern Costa Rica (Brasse et al. 2009) is consistent with $0.9 \pm 0.5\%$ melt, depending on temperature and melt H_2O content. Extensive melting may occur in the regions of extremely high conductivity (1 S/m) beneath the Bolivian Orocline (Brasse and Eydam 2008), with melt fraction in the order of 5–15%. Alternatively, these anomalies may be produced by lower fractions of very water-rich melts or by the presence of some highly conductive, saline fluids.

Conclusions

We show that the effect of water on the electrical conductivity of basaltic melt is significantly larger than previously assumed. For water contents above 6 wt%, the conductivity of hydrous basalt melts almost approaches that of carbonatites in the mantle. Dissolved CO_2 in the order of 0.5 wt%, on the other hand, does not have any

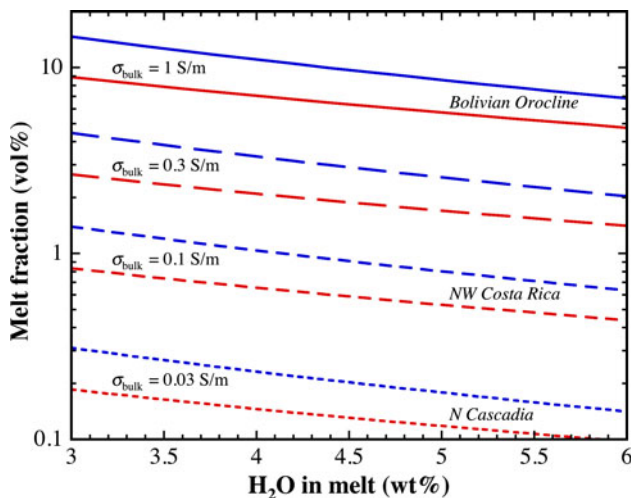


Fig. 9 Contour plots of electrical conductivity for various melt fractions and melt H₂O contents in a partially molten mantle wedge of a subduction zone (red for 1,673 K and blue for 1,573 K), assuming the Hashin and Shtrikman (1962) upper bound. Also indicated are locations where the highest conductivity from MT studies is 0.03, 0.1, and 1 S/m (Soyer and Unsworth 2006; Brasse and Eydam 2008; Brasse et al. 2009)

detectable effect on the electric conductivity of basaltic melt.

Our data suggest that between 0.3 and 2% of hydrous basaltic melt can account for the observed electrical conductivity in the LVZ, or at least in the upper LVZ (70–110 km depths). The melt should be segregated into tube-like structures, elongated in the direction of plate spreading, which would be consistent with both the observed electric and seismic anisotropy. The conductivity model in this work can also be applied to constrain the degree of melting at subduction zones.

Acknowledgments We thank Hubert Schulze and Uwe Dittmann for sample preparation and Sven Linhardt for assistance in the conductivity experiments. Constructive reviews by F. Gaillard, A. Pommier, and an anonymous referee improved the manuscript. Discussions with B. Poe were beneficial.

References

Angell CA (1991) Relaxation in liquids, polymers and plastic crystals—strong/fragile patterns and problems. *J Non-Cryst Solids* 131–133:13–31

Arcay D, Tric E, Doin M-P (2005) Numerical simulations of subduction zones: effect of slab dehydration on the mantle wedge dynamics. *Phys Earth Planet Inter* 149:133–153

Archie GE (1942) The electrical resistivity log as an aid in determining some reservoir characteristics. *Trans Am Inst Min Metall Pet Eng* 146:54–62

Baba K, Chave AD, Evans RL, Hirth G, Mackie RL (2006) Mantle dynamics beneath the East Pacific Rise at 17°S: insights from the Mantle Electromagnetic and Tomography (MELT) experiment. *J Geophys Res* 111:B02101. doi:10.1029/2004JB003598

Barsoukov E, Macdonald JR (2005) Impedance spectroscopy. Wiley, New Jersey

Behrens H, Kappes R, Heitjans P (2002) Proton conduction in glass—an impedance and infrared spectroscopic study on hydrous BaSi₂O₅ glass. *J Non-Cryst Solids* 306:271–281

Behrens H, Zhang Y, Xu Z (2004) H₂O diffusion in dacitic and andesitic melts. *Geochim Cosmochim Acta* 68:5139–5150

Bell DR, Rossman GR, Moore RO (2004) Abundance and partitioning of OH in a high-pressure magmatic system: megacrysts from the Monastery kimberlite, South Africa. *J Petrol* 45:1539–1564

Brasse H, Eydam D (2008) Electrical conductivity beneath the Bolivian Orocline and its relation to subduction processes at the South American continental margin. *J Geophys Res* 113:B07109. doi:10.1029/2007JB005142

Brasse H, Kapinos G, Mütschard L, Alvarado GE, Worzewski T, Jegen M (2009) Deep electrical resistivity structure of north-western Costa Rica. *Geophys Res Lett* 36:L02310. doi:10.1029/2008GL036397

Brearely M, Montana A (1989) The effect of CO₂ on the viscosity of silicate liquids at high pressure. *Geochim Cosmochim Acta* 53:2609–2616

Brooker RA, Kohn SC, Holloway JR, McMillan PF (2001) Structural controls on the solubility of CO₂ in silicate melts. Part I: bulk solubility data. *Chem Geol* 174:225–239

Cervantes P, Wallace PJ (2003) Role of H₂O in subduction-zone magmatism: new insights from melt inclusions in high-Mg basalts from central Mexico. *Geology* 31:235–238

Constable S (2006) SEO3: a new model of olivine electrical conductivity. *Geophys J Int* 166:435–437

Dingwell DB, Webb SL (1990) Relaxation in silicate melts. *Eur J Mineral* 2:427–449

Dixon JE, Stolper E, Delaney JR (1988) Infrared spectroscopic measurements of CO₂ and H₂O in Juan de Fuca Ridge basaltic glasses. *Earth Planet Sci Lett* 90:87–104

Ernsberger FM (1980) The role of molecular water in the diffusive transport of protons in glasses. *Phys Chem Glasses* 21:146–149

Evans RL, Hirth G, Baba K, Forsyth D, Chave A, Mackie R (2005) Geophysical evidence from the MELT area for compositional controls on oceanic plates. *Nature* 437:249–252

Falloon TJ, Green DH, Danyushevsky LV, McNeill AW (2008) The composition of near-solidus partial melts of fertile peridotite at 1 and 1.5 GPa: implications for the petrogenesis of MORB. *J Petrol* 49:591–613

Fulcher GS (1925) Analysis of recent measurements of the viscosity of glasses. *J Am Ceram Soc* 8:339–355

Gaetani GA, Grove TL (1998) The influence of water on melting of mantle peridotite. *Contrib Mineral Petrol* 131:323–346

Gaillard F (2004) Laboratory measurements of electrical conductivity of hydrous and dry silicic melts under pressure. *Earth Planet Sci Lett* 218:215–228

Gaillard F, Iacono-Marziano G (2005) Electrical conductivity of magma in the course of crystallization controlled by their residual liquid composition. *J Geophys Res* 110:B06204. doi:10.1029/2004JB003282

Gaillard F, Schmidt B, Mackwell S, McCammon C (2003) Rate of hydrogen-iron redox exchange in silicate melts and glasses. *Geochim Cosmochim Acta* 67:2427–2441

Gaillard F, Malki M, Iacono-Marziano G (2008) Carbonatite melts and electrical conductivity in the asthenosphere. *Science* 322:1363–1365

Giordano D, Dingwell DB (2003) Viscosity of hydrous Etna basalt: implications for Plinian-style basaltic eruptions. *Bull Volcanol* 65:8–14

Glover PWJ, Hole MJ, Pous J (2000) A modified Archie's law for two conducting phases. *Earth Planet Sci Lett* 180:369–383

- Green DH, Hibberson WO, HSTC O'Neill (2008) Clarification of the influence of water on mantle wedge melting. *Geochim Cosmochim Acta* 72:A325
- Grove TL, Parman SW, Bowring SA, Price RC, Baker MB (2002) The role of an H₂O-rich fluid component in the generation of primitive basaltic andesites and andesites from the Mt. Shasta region, N California. *Contrib Mineral Petrol* 142:275–396
- Grove TL, Chatterjee N, Parman SW, Medard E (2006) The influence of H₂O on mantle wedge melting. *Earth Planet Sci Lett* 249:74–89
- Hashin Z, Shtrikman S (1962) A variational approach to the theory of the effective magnetic permeability of multiphase materials. *J Appl Phys* 33:3125–3131
- Haven Y, Verkerk B (1965) Diffusion and electrical conductivity of sodium ions in sodium silicate glasses. *Phys Chem Glasses* 6:38–45
- Heinemann I, Frischat GH (1993) The sodium transport mechanism in Na₂O-2SiO₂ glass determined by the Chemla experiment. *Phys Chem Glasses* 34:255–260
- Hirschmann MM (2010) Partial melt in the oceanic low velocity zone. *Phys Earth Planet Inter* 179:60–71
- Hirschmann MM, Tenner T, Aubaud C, Withers AC (2009) Dehydration melting of nominally anhydrous mantle: the primacy of partitioning. *Phys Earth Planet Inter* 176:54–68
- Hodges FN (1974) The solubility of H₂O in silicate melts. *Carnegie Inst Wash Yearb* 73:251–255
- Ingrin J, Blanchard M (2006) Diffusion of hydrogen in minerals. *Rev Mineral Geochem* 62:291–320
- Karato S-I (2006) Remote sensing of hydrogen in Earth's mantle. *Rev Mineral Geochem* 62:343–375
- Kawakatsu H, Kumar P, Takei Y, Shinohara M, Kanazawa T, Araki E, Suyehiro K (2009) Seismic evidence for sharp lithosphere-asthenosphere boundaries of oceanic plates. *Science* 324:499–502
- Khitarov NI, Slutsky AB, Pugin VA (1970) Electrical conductivity of basalts at high T-P and phase transitions under upper mantle conditions. *Phys Earth Planet Inter* 3:334–342
- Kohn SC, Grant KJ (2006) The partitioning of water between nominally anhydrous minerals and silicate melts. *Rev Mineral Geochem* 62:231–241
- Konschak A (2008) CO₂ in Silikatschmelzen. Ph.D. Dissertation, Universität Bayreuth
- Kushiro I (1972) Effect of water on the composition of magmas formed at high pressures. *J Petrol* 13:311–334
- Lange RA, Carmichael ISE (1987) Densities of Na₂O-K₂O-CaO-MgO-FeO-Fe₂O₃-Al₂O₃-TiO₂-SiO₂ liquids: new measurements and derived partial molar properties. *Geochim Cosmochim Acta* 51:2931–2946
- Liu X, O'Neill HSC, Berry AJ (2006) The effect of small amounts of H₂O, CO₂ and Na₂O on the partial melting of spinel lherzolite in the system CaO-MgO-Al₂O₃-SiO₂ ± H₂O ± CO₂ ± Na₂O at 1.1 GPa. *J Petrol* 47:409–434
- Lowrie W (1997) *Fundamentals of geophysics*. Cambridge University Press, Cambridge, UK p 206
- Lowry RK, Henderson P, Nolan J (1982) Tracer diffusion of some alkali, alkaline-earth and transition element ions in a basaltic and an andesitic melt, and the implications concerning melt structure. *Contrib Mineral Petrol* 80:254–261
- Manning CE (2004) The chemistry of subduction-zone fluids. *Earth Planet Sci Lett* 223:1–16
- Michael P (1995) Regionally distinctive sources of depleted MORB: evidence from trace elements and H₂O. *Earth Planet Sci Lett* 131:301–320
- Mierdel K, Keppler H, Smyth JR, Langenhorst F (2007) Water solubility in aluminous orthopyroxene and the origin of Earth's asthenosphere. *Science* 315:364–368
- Mungall JE (2002) Empirical models relating viscosity and tracer diffusion in magmatic silicate melts. *Geochim Cosmochim Acta* 66:125–143
- Murase T, McBirney AR (1973) Properties of some common igneous rocks and their melts at high temperatures. *Geol Soc Am Bull* 84:3563–3592
- Ni H, Zhang Y (2008) H₂O diffusion models in rhyolitic melt with new high pressure data. *Chem Geol* 250:68–78
- Ni H, Liu Y, Wang L, Zhang Y (2009a) Water speciation and diffusion in haploandesitic melts at 743–873 K and 100 MPa. *Geochim Cosmochim Acta* 73:3630–3641
- Ni H, Behrens H, Zhang Y (2009b) Water diffusion in dacitic melt. *Geochim Cosmochim Acta* 73:3642–3655
- Ni H, Keppler H, Manthilake MAGM, Katsura T (2011) Electrical conductivity of dry and hydrous NaAlSi₃O₈ glasses and liquids at high pressures. *Contrib Mineral Petrol* 161. doi:10.1007/s00410-011-0608-5
- Ochs FA, Lange RA (1997) The partial molar volume, thermal expansivity, and compressibility of H₂O in NaAlSi₃O₈ liquid: new measurements and an internally consistent model. *Contrib Mineral Petrol* 129:155–165
- Ohlhorst S, Behrens H, Holtz F (2001) Compositional dependence of molar absorptivities of near-infrared OH- and H₂O bands in rhyolitic to basaltic glasses. *Chem Geol* 174:5–20
- Pfeiffer T (1998) Viscosities and electrical conductivities of oxidic glass-forming melts. *Solid State Ionics* 105:277–287
- Poe BT, Romano C, Nestola F, Smyth JR (2010) Electrical conductivity anisotropy of dry and hydrous olivine at 8 GPa. *Phys Earth Planet Inter* 181:103–111
- Pommier A, Gaillard F, Pichavant M, Scaillet B (2008) Laboratory measurements of electrical conductivities of hydrous and dry Mount Vesuvius melts under pressure. *J Geophys Res* 113:B05205. doi:10.1029/2007JB005269
- Pommier A, Gaillard F, Malki M, Pichavant M (2010a) Methodological re-evaluation of the electrical conductivity of silicate melts. *Am Mineral* 95:284–291
- Pommier A, Gaillard F, Pichavant M (2010b) Time-dependent changes of the electrical conductivity of basaltic melts with redox state. *Geochim Cosmochim Acta* 74:1653–1671
- Presnall DC, Simmons CL, Porath H (1972) Changes in electrical conductivity of a synthetic basalt during melting. *J Geophys Res* 77:5665–5672
- Saal AE, Hauri EH, Langmuir CH, Perfit MR (2002) Vapour undersaturation in primitive mid-ocean-ridge basalt and the volatile content of Earth's upper mantle. *Nature* 419:451–455
- Salter VJM, Hart SR (1989) The hafnium paradox and the role of garnet in the source of mid-ocean-ridge basalts. *Nature* 342:420–422
- Salter VJM, Stracke A (2004) Composition of the depleted mantle. *Geochem Geophys Geosys* 5:Q05B07. doi: 10.1029/2003GC000597
- Shaw HR (1963) Obsidian-H₂O viscosities at 1000 and 2000 bars in the temperature range 700° to 900°C. *J Geophys Res* 68:6337–6343
- Shen Y, Forsyth DW (1995) Geochemical constraints on initial and final depths of melting beneath mid-ocean ridges. *J Geophys Res* 100:2211–2237
- Sisson TW, Layne GD (1993) H₂O in basalt and basaltic andesite glass inclusions from four subduction-related volcanoes. *Earth Planet Sci Lett* 117:619–635
- Soyer W, Unsworth M (2006) Deep electrical structure of the northern Cascadia (British Columbia, Canada) subduction zone: implications for the distribution of fluids. *Geology* 34:53–56
- The MELT Seismic Team (1998) Imaging the deep seismic structure beneath a mid-ocean ridge: the MELT experiment. *Science* 280:1215–1218

- Tyburczy JA, Waff HS (1983) Electrical conductivity of molten basalt and andesite to 25 kilobars pressure: geographical significance and implications for charge transport and melt structure. *J Geophys Res* 88:2413–2430
- van Keken PE, Kiefer B, Peacock SM (2002) High-resolution models of subduction zones: implications for mineral dehydration reactions and the transport of water into the deep mantle. *Geochem Geophys Geosys* 3:1056. doi:[10.1029/2001GC000256](https://doi.org/10.1029/2001GC000256)
- Waff HS, Weill DF (1975) Electrical conductivity of magmatic liquids: effects of temperature, oxygen fugacity and composition. *Earth Planet Sci Lett* 28:254–260
- Wang D, Mookherjee M, Xu Y, Karato S-I (2006) The effect of water on the electrical conductivity of olivine. *Nature* 443:977–980
- Watson EB (1979) Diffusion of cesium ions in H₂O-saturated granitic melt. *Science* 205:1259–1260
- Whittington A, Richet P, Holtz F (2000) Water and the viscosity of depolymerized aluminosilicate melts. *Geochim Cosmochim Acta* 64:3725–3736
- Workman RK, Hart SR (2005) Major and trace element composition of the depleted MORB mantle (DMM). *Earth Planet Sci Lett* 231:53–72
- Xu Y, Poe BT, Shankland TJ, Rubie DC (1998) Electrical conductivity of olivine, wadsleyite, and ringwoodite under upper-mantle conditions. *Science* 280:1415–1418
- Yamashita S, Kitamura T, Kusakabe M (1997) Infrared spectroscopy of hydrous glasses of arc magma compositions. *Geochem J* 31:169–174
- Yoshino T, Matsuzaki T, Yamashita S, Katsura T (2006) Hydrous olivine unable to account for conductivity anomaly at the top of the asthenosphere. *Nature* 443:973–976
- Yoshino T, Laumonier M, McIsaac E, Katsura T (2010) Electrical conductivity of basaltic and carbonatite melt-bearing peridotites at high pressures: implications for melt distribution and melt fraction in the upper mantle. *Earth Planet Sci Lett* 295:593–602
- Zhang Y, Ni H (2010) Diffusion of H, C, and O components in silicate melts. *Rev Mineral Geochem* 72:171–225
- Zhang Y, Stolper EM (1991) Water diffusion in basaltic melts. *Nature* 351:306–309
- Zhang Y, Stolper EM, Wasserburg GJ (1991) Diffusion of water in rhyolitic glasses. *Geochim Cosmochim Acta* 55:441–456
- Zhang Y, Ni H, Chen Y (2010) Diffusion data in silicate melts. *Rev Mineral Geochem* 72:311–408